

Lawrence Berkeley National Laboratory

Lawrence Berkeley National Laboratory

Title

Compressive Phase Contrast Tomography

Permalink

<https://escholarship.org/uc/item/2cr546zi>

Author

Maia, Filipe

Publication Date

2010-09-02

Compressive Phase Contrast Tomography

F. Maia^a, A. MacDowell^b, S. Marchesini^b, H. A. Padmore^a, D. Y. Parkinson^a, J. Pien^d, A. Schirotzek^a, C. Yang^c.

^a National Energy Research Scientific Computing Center, Lawrence Berkeley National Laboratory, Berkeley, California, 94720, USA ^b Advanced Light Source, Lawrence Berkeley National Laboratory, Berkeley, CA, USA; ^c Computational Research Division, Lawrence Berkeley National Laboratory, Berkeley, CA, USA; ^d CUDA consultant, www.jackpien.com

ABSTRACT

When x-rays penetrate soft matter, their phase changes more rapidly than their amplitude. Interference effects visible with high brightness sources creates higher contrast, edge enhanced images. When the object is piecewise smooth (made of big blocks of a few components), such higher contrast datasets have a sparse solution. We apply basis pursuit solvers to improve SNR, remove ring artifacts, reduce the number of views and radiation dose from phase contrast datasets collected at the Hard X-Ray Micro Tomography Beamline at the Advanced Light Source. We report a GPU code for the most computationally intensive task, the gridding and inverse gridding algorithm (non uniform sampled Fourier transform).

Keywords: Compressive Sensing, non uniform FFT, Radon transform, GPU

1. INTRODUCTION

Phase contrast tomography allows the imaging of light materials that would otherwise be transparent to x-rays, and obtaining edge enhancement at higher SNR for the same dose^{1,2}. Further dose reduction is expected from the application of compressive sensing reconstruction techniques. This is what we set out to do in this paper.

The refractive index of X-rays passing through light materials is very close to a real number; when written in the form: $n = 1 - \delta + i\beta$, δ is one to 3 orders of magnitudes larger than β (depending on the energy of the X-rays); exploiting the refractive contrast seems obvious.

While it is not possible to observe phases, experimental methods exist to observe the Laplacian of the phase changes induced by propagation through an object. By rotating the object around an axis, one can collect a series of such projections. Standard tomographic processing of the data yields the laplacian of the object in the three dimensional space.²

The phase contrast mechanism is especially useful for defining the boundaries between composite objects. If the sample is made of large blocks of components, the boundaries will be thin and far from each other. In other words, the solution will be sparse.

We tested this concept using experimental phase contrast data from 20 micron glass spheres at the tomography beamline 8.3.2 at the Advanced Light Source, Lawrence Berkeley National Lab. The setup is similar to standard tomography procedures⁵ in that samples are rotated in a monochromatic X-ray beam and the transmitted X-rays are imaged via a scintillator, magnifying lens and a digital camera to give an effective voxel size in the reconstructed three-dimensional image of 1.8 μm .

Background normalized images are shown in Fig. 1, along with their difference showing the propagation based phase contrast enhancement, and the corresponding sinogram. Significant artifacts arise from the residual fluctuations in the illuminating beam due to vibrations and the high power beam impinging on a crystal monochromator. Defective detector elements (e.g. dead pixels in a CCD) with non-linear responses to incoming intensity will appear in the reconstructions as sharp rings with a width of one pixel. Similar artifacts also arise

Further author information: (Send correspondence to S.M.)
S.M.: E-mail: smarchesini@lbl.gov

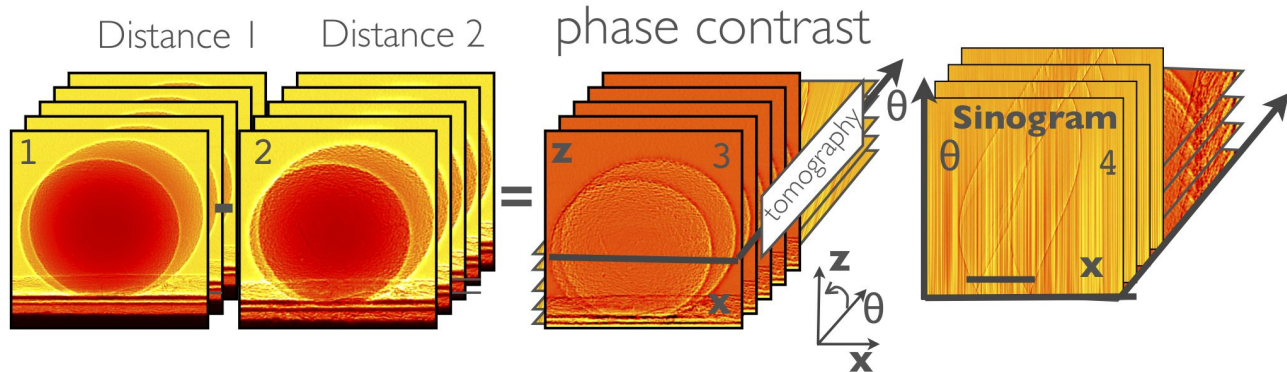


Figure 1. Propagation based phase contrast and tomography of two two glass balls placed in the microtomography beamline 8.3.2. From left to right: (1) projection radiograph at short distance from the sample, (2) same as (1) but with the detector 1 m. downstream. (3) difference between (1) and (2), (4) sinogram.

from dusty or damaged scintillator screens. Miscalibrated detector pixels, e.g. due to beam instabilities not completely taken into account by a normalization correction, give rise to wider and less marked rings.⁶

To improve the reconstruction we employed a 3rd order polynomial fit to smooth the sinogram and reduce the ringing artifacts. Increasing the order of the polynomial beyond 3 did not improve the image further (Fig. 2).

We formulated the final reconstruction problem as an L1-minimization problem, i.e.

$$\begin{aligned} & \min \|x\|_1 \\ & \text{subject to } \|\text{filter}(\text{Radon}\{x\} - \text{data})\|_2 < \epsilon \end{aligned}$$

where x is the phase contrast image to be reconstructed and filter is a polynomial interpolation operator designed to reduce the ringing artifact in the reconstruction, and ϵ is a regularization parameter we choose in advance. We solve the L1-minimization problem by using the SPGL1 software developed by E. van den Berg and M. P. Friedlander [1]. The software requires us to provide a function to perform $y = \text{Radon}\{x\}$. Due to the large volume of data produced by at beam line (BL.8.3.2) at the Advanced Light Source, we would like perform phase contrast tomographic reconstruction in real time.

2. FAST RADON TRANSFORM

Fast Radon and inverse Radon transforms form the computational kernels of many image reconstruction algorithms. The 2D Radon transform of an image x can be implemented in a number of ways. One of the most efficient ways to perform $\text{Radon}\{x\}$ is to first perform a 2D FFT of x on a regular grid, and then interpolate the transform onto a polar grid before 1D inverse Fourier transforms are applied to interpolated points along the same radial lines.

The interpolation between the Cartesian and polar grid is the key step in this procedure. It can be carried out using a “gridding” algorithm that maintains the desired accuracy with low computational complexity. The gridding algorithm essentially allows us to perform a non-uniform FFT.

The gridding operation requires the convolution between irregular samples and a kernel calculated at regular sample position and vice versa (Fig. 5 and³).

A fast GPU implementation requires dividing the problem into each blocks with similar computational loads. Our approach starts with one bin containing all the points, and then recursively divides the most computationally intensive bin into four equally sized bins. The computational intensity is estimated by multiplying the number

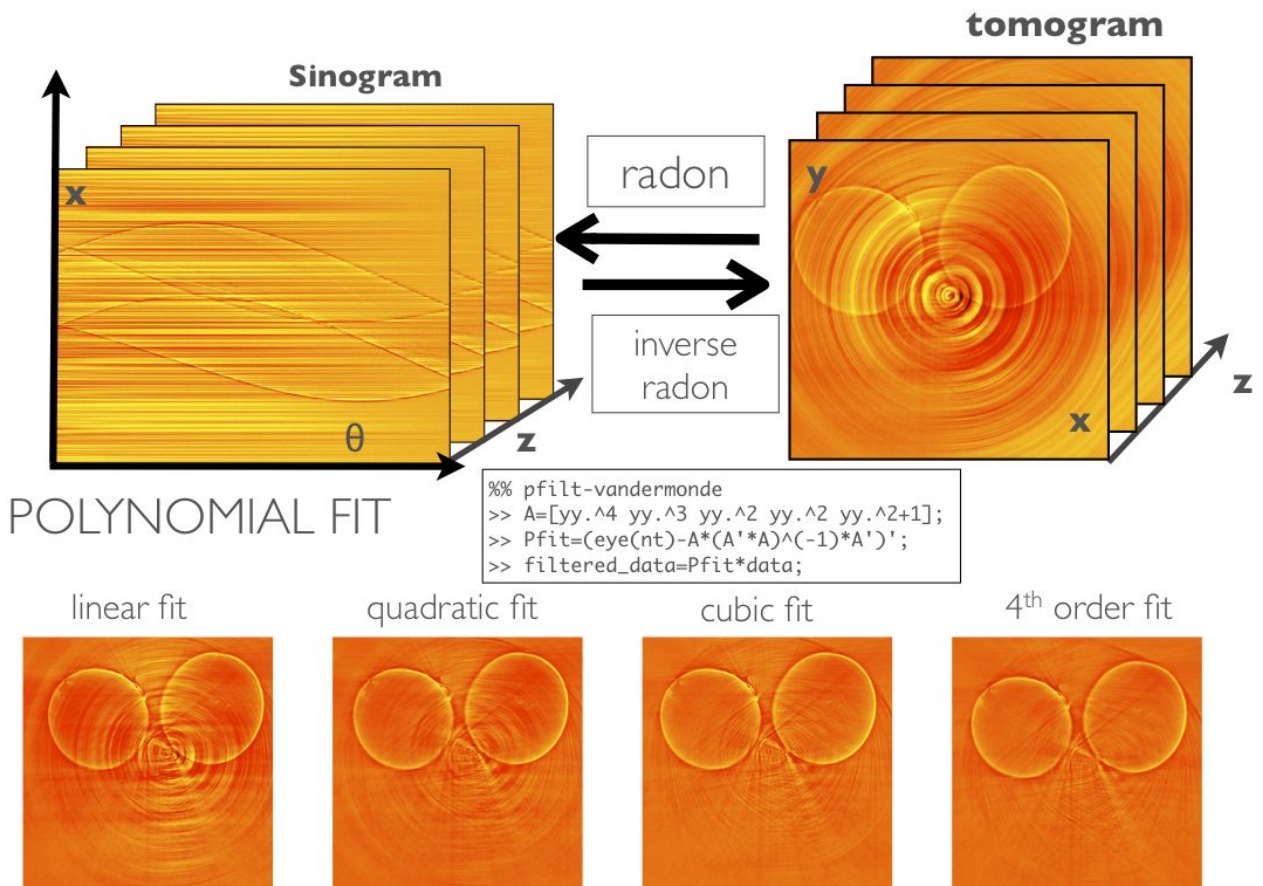


Figure 2. Significant artifact due to residual fluctuations in the illuminating beam due to vibrations and the high power beam impinging on a crystal monochromator. Comparison of image quality using different filters (polynomial subtraction) (Fig. 2).

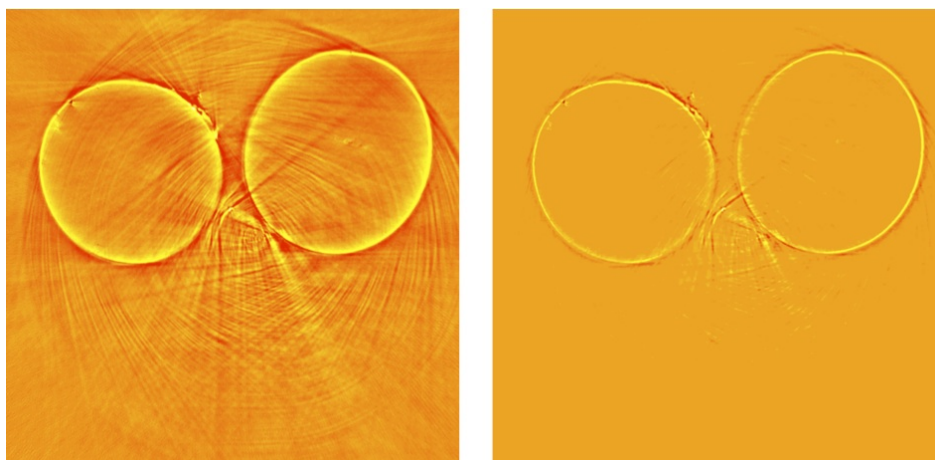


Figure 3. Comparison of the reconstruction using a filter and using SPGL1 basis pursuit solver with the same filter.

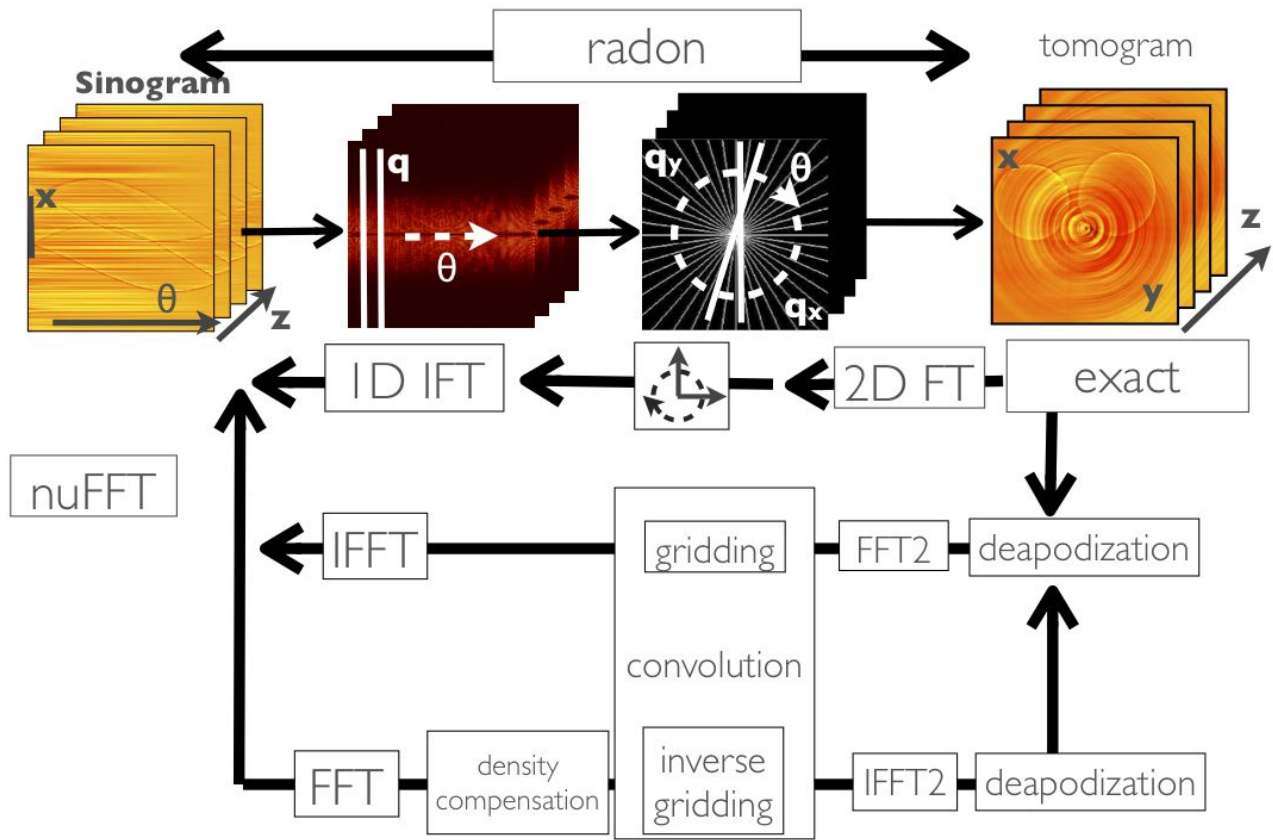


Figure 4. Fast Radon and inverse Radon transforms implemented on a Tesla GPU computing engine.

The Gridding Algorithm

Inverse gridding: Convolve Kaiser Bessel (KB) kernel from regular samples (x_r, y_r) to regular grid points (x_i, y_i)

$$G_r(x_i, y_i) = \sum_{x_r, y_r} \frac{1}{D(x_i, y_i)} G_i(x_i, y_i) K(x_i - x_r, y_i - y_r)$$

Gridding: Convolve KB kernel from irregular samples (x_i, y_i) to regular grid points (x_r, y_r) .

$$G_i(x_i, y_i) = \sum_{x_r, y_r} G_r(x_r, y_r) K(x_r - x_i, y_r - y_i)$$

Density compensation:

$$D_i(x_i, y_i) = \sum_{i,j} K(x_i - x_j, y_i - y_j)$$

Deapodization:

$$d = \frac{1}{FFT K(x_r, y_r)} \text{ constant}$$

Figure 5. Fast Radon and inverse Radon transforms implemented on a Tesla GPU computing engine.

of samples in the bin by the number of grid points in the bin. For the calculation in the GPU we assign one thread block per bin. The calculation strategy depends on the number of samples in the bin. When the number of samples does not fit in shared memory we assign all threads to each grid point and access the samples in a coalesced way. When it does fit in shared memory we assign one thread per grid point.

Further details of the code will be described in the future. Preliminary tests indicate 50x speedup on a Tesla GPU C1060 compared to a fast CPU (e.g.: 3 msec for the FFTs, 6 msec for gridding+inverse gridding for a 1024x1024 grid sampled with 180 angles, 1024 pixels per angle).

2.1 Conclusions

In summary we implemented a GPU-accelerated compressive phase contrast tomography reconstruction using Basis Pursuit solvers for the high throughput tomography beamline at the Advanced Light Source. The reconstruction procedure was used to remove ring artifacts but it is expected to also enable lower dose or smaller datasets for similar image quality as shown for simple tomographic datasets.

Acknowledgments

This work was supported by the Laboratory Directed Research and Development Program of Lawrence Berkeley National Laboratory under U.S. Department of Energy Contract No. DE-AC02-05CH11231. We acknowledge the use of the X-ray synchrotron micro-tomography beam line (8.3.2) at the Advanced Light Source at LBNL, supported by the Office of Science of the Department of Energy. Part of the work was developed using Jacket GPU toolbox for matlab provided by Accelerereyes.

REFERENCES

- [1] Nugent, K. A. "Coherent Methods in the X-ray Sciences", *Advances in Physics* 59, 1-99, 2010.
- [2] Paganin, D.M. "Coherent X-ray Optics", Oxford University Press, Oxford, (2006).
- [3] Jackson, J. I. Meyer, C. H. Nishimura, D. G. "Selection of a Convolution Function for Fourier Inversion using Gridding." *IEEE Trans. Med. Imag.* 10(3), 473- (1991).
- [4] van den Berg, E. and Friedlander, M. P. "Probing the Pareto frontier for basis pursuit solutions", *SIAM J. on Sci. Comp.* 31, 890-912, (2008).
- [5] Kinney, J.H. Nichols, M.C. X-ray tomographic microscopy using synchrotron radiation. *Annu Rev Mater Sci* 22, 121 (1992).
- [6] Münch, B. Trtik, P. Marone, F. and Stampanoni, M. "Stripe and ring artifact removal with combined wavelet-Fourier filtering", *Optics Express* 17(10), pp. 8567-8591 (2009).